

AIRS Deconvolution and Translation from the AIRS to CrIS IR Sounders

**** DRAFT ****

Howard E. Motteler
L. Larrabee Strow

UMBC Atmospheric Spectroscopy Lab
Joint Center for Earth Systems Technology

June 4, 2017

1 Introduction

Upwelling infrared radiation as measured by the AIRS [1] and CrIS [2, 6] sounders is a significant part of the long term climate record. We would like to treat this as a single data set and often want to compare radiances, for example in the analysis of simultaneous nadir overpasses (SNOs) for sounder calibration or validation. However the instruments have different spectral resolutions, channel response functions, and band spans. As a step in addressing this problem we consider the translation of channel radiances from AIRS to standard resolution CrIS.

Translation from AIRS to CrIS involves more than basic resampling. AIRS is a grating spectrometer with a distinct response function for each channel determined by the focal plane geometry, while CrIS is a Michelson interferometer with a sinc response function, after calibration and corrections. In section 2 we show how to take advantage of our detailed knowledge of the AIRS spectral response functions (SRFs) and their overlap to deconvolve channel radiances to a resolution-enhanced intermediate representation, typically a 0.1 cm^{-1} grid, the approximate resolution of the tabulated AIRS SRFs.

This intermediate representation can then be reconvolved, for example to an idealized grating instrument with a generalized Gaussian response

function or to the CrIS user grid with a sinc basis. Section 3 gives details and validation tests for the AIRS to CrIS translation. In section ?? we consider alternate translations, including conventional interpolation and direct regression from AIRS to CrIS. Section 5 gives some applications and conclusions.

2 AIRS Deconvolution

The AIRS spectral response functions model channel response as a function of frequency and associate channels with nominal center frequencies. Each AIRS channel i has an associated spectral response function or SRF $\sigma_i(v)$ such that the channel radiance $c_i = \int \sigma_i(v)r(v) dv$, where r is radiance at frequency v . The center or peak of σ_i is the nominal channel frequency.

Figure 1 shows typical AIRS SRFs from the low and high ends of the band. Note the significant overlap in the wings. This can allow for a deconvolution to recover resolution beyond that of the response functions considered individually. The SRFs are not necessarily symmetrical, especially at the high end of the band. The dashed line on top of the third SRF is a fit of a generalized Gaussian, which we consider in more detail later in this section. Figure 2 shows channel spacing and resolving power for the AIRS L1c channel set [?]. The variable channel spacing and resolving power are due to the modular structure of the focal plane. Although not entirely regular—that is, not a simple function of frequency—the L1c channel set is more regular than the L1b channel set from which it is derived, and we mainly consider the L1c set here.

Suppose we have n channels and a frequency grid \vec{v} of k points spanning the union of the domains of the functions σ_i . The grid step size for our applications is often 0.0025 cm^{-1} , the kcarta resolution [4]. Let S_k be an $n \times k$ array such that $s_{i,j} = \sigma_i(v_j)/w_i$, where $w_i = \sum_j \sigma_i(v_j)$, that is where row i is $\sigma_i(v)$ tabulated at the grid \vec{v} and normalized so the row sum is 1. If the channel centers are in increasing order S_k is banded, and if they are not too close (as is the case for a few of the L1b channels) the rows are linearly independent. S_k is a linear transform whose domain is radiance at the grid \vec{v} and whose range is channel radiances. If r is radiance at the grid \vec{v} , then $c = S_k r$ gives a good approximation of the channel radiances $c_i = \int \sigma_i(v)r(v) dv$. In practice this is how we convolve kcarta or other high resolution calculated radiances to get AIRS channel radiances, for example for reference truth or “true AIRS” for the tests shown here.

For the AIRS to CrIS and other translations we are mainly interested

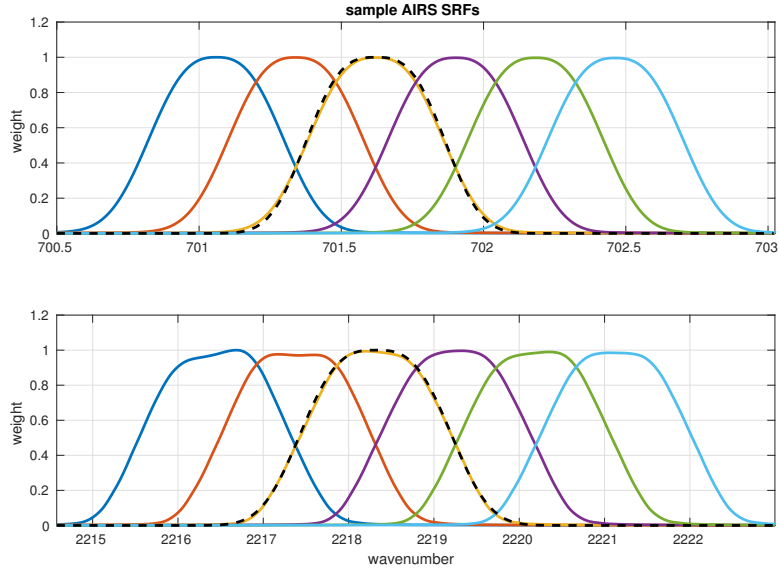


Figure 1: sample AIRS spectral response functions from the low and high ends of the band. The dashed line is a generalized Gaussian function.

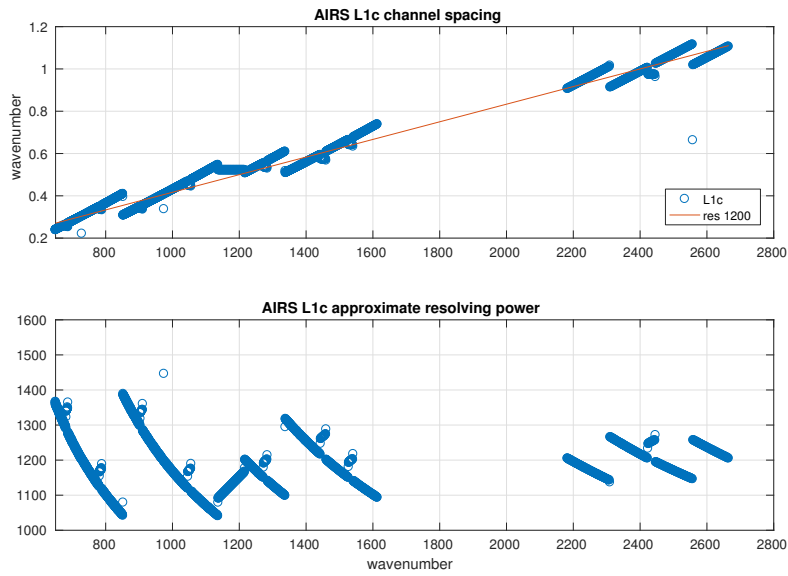


Figure 2: AIRS L1c channel spacing and derived resolving power.

in the transform S_b for SRFs at an intermediate resolution, typically 0.1 cm^{-1} . This is the approximate resolution of the SRF measurements and convenient for reconvolution to the CrIS user grid. So let $\vec{v}_b = v_1, v_2, \dots, v_m$ be a 0.1 cm^{-1} grid spanning the domains of the functions σ_i . Similar to S_k , let S_b be an $n \times m$ array where row i is $\sigma_i(v)$ tabulated at the \vec{v}_b grid, with rows normalized to 1. If r is radiance at the \vec{v}_b grid, then $c = S_b r$ is still a reasonable approximation of $\int \sigma_i(v) r(v) dv$.

For our application we want to start with c and find r , that is to deconvolve c by solving $S_b r = c$ for r . Since $m < k$, the system is underdetermined, but we can take r as $r_0 = S_b^{-1} c$ where S_b^{-1} is the Moore-Penrose pseudoinverse [?] of S_b . This has the key property of finding r_0 such that $\|r_0\|_2 \leq \|r_j\|_2$ for all r_j satisfying $S_b r_j = c$. The condition number for S_b built from the L1c channels is $\|S_b\|_2 \|S_b^{-1}\|_2 = 115$, which is acceptable.

Although our main goal is to reconvolve the 0.1 cm^{-1} intermediate representation to the CrIS or other user grids, we first compare the deconvolved radiances with reference truth from a direct convolution to intermediate grid. The choice of response functions for this direct convolution is not obvious, since the deconvolution is undoing—at least to some extent—the effects of the AIRS SRF convolutions. We use a generalized Gaussian of the form

$$w = \exp \left(- \left(\frac{(x - v_0)^2}{2c^2} \right)^{1.5} \right)$$

where $c = \text{FWHM}/2.355$ and v_0 is the desired channel center. The exponent 1.5 was chosen to give an approximate match to AIRS SRFs with the same FWHM and channel centers, though without the fine structure and variation of the latter. Figure 1 shows two such functions paired with AIRS SRFs with the same FWHM and centers. We used this function for the 0.1 cm^{-1} intermediate grid with $\text{FWHM} = v_i/2000$ where v_i are the grid frequencies. This represents a hypothetical grating spectrometer with a resolving power of 2000, oversampled to the 0.1 cm^{-1} grid.

The AIRS deconvolution gives a modest resolution enhancement, at the cost of added artifacts and noise. Figure 3 shows details of karta, direct convolution to the 0.1 cm^{-1} grid (“gauss”), deconvolution, and AIRS spectra for fitting profile 1 [3, 5]. In the first subplot we see the deconvolution is capturing some of the fine structure in the karta data that is present in the direct convolution but not in the AIRS data. In the second subplot we see the deconvolution (and direct convolution) resolving a pair of close lines that are not resolved at the AIRS L1c resolution. But we also see some ringing that is not present in the direct convolution. Figure 4 shows the

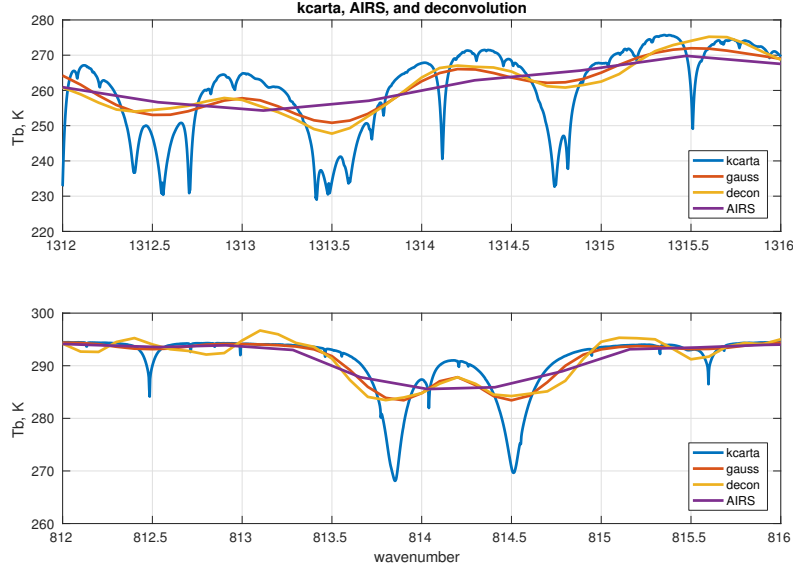


Figure 3: details from fitting profile 1 for kcarta, direct convolution to the 0.1 cm^{-1} grid ("gauss"), deconvolved AIRS, and true AIRS.

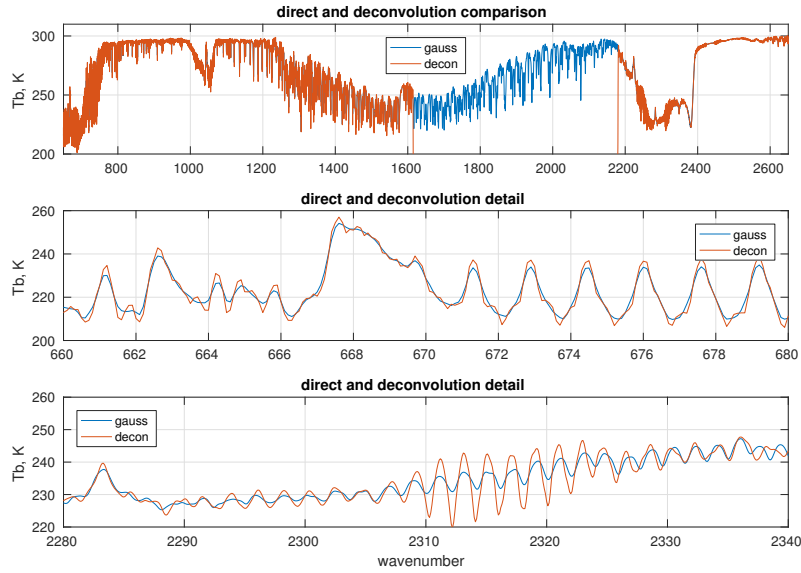


Figure 4: spectra from fitting profile 1 for direct convolution to the 0.1 cm^{-1} grid ("gauss") and deconvolved AIRS

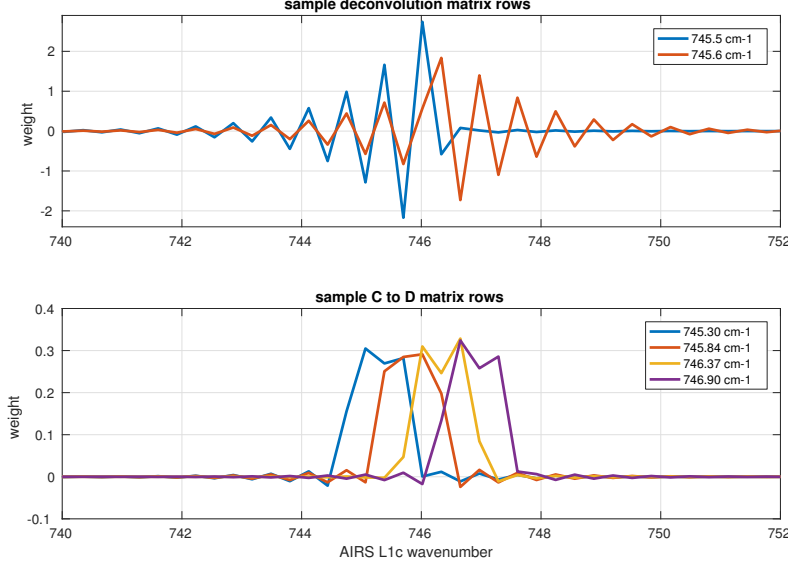


Figure 5: sample adjacent rows for the deconvolution and L1c to L1d transforms

full spectra from fitting profile 1, along with sample details from the low and high ends of the band, for the deconvolution and direct convolution to the intermediate grid. In the details we see some overshoot and ringing in the deconvolution. But we do not propose using the deconvolved radiances directly, they are an intermediate step in reconvolution to a lower resolution.

Figure 5 shows a pair of typical adjacent rows of the deconvolution matrix S_b^{-1} in the first subplot. Row i of S_b^{-1} is the weights applied to L1c channel radiances to synthesize the deconvolved radiance r_i at the intermediate grid frequency v_i . The oscillation simply means we are taking the closest AIRS channel, subtracting weighted values for channels ± 1 step away, adding weighted values for channels ± 2 steps away, and so on, with the weights decreasing quickly as we move away from v_i , with eight to ten L1c channels making a significant contribution to each deconvolution grid point.

The second subplot shows four adjacent rows of the matrix $S_d \cdot S_b^{-1}$, which takes L1c to L1d channel radiances. (The L1d radiances are discussed in a later section; here they are of interest mainly as a typical reconvolution.) Both matrices are banded but the bands are narrower in the second, with three to five L1c channels contributing significantly to each L1d channel. The range of influence is significant since for example we may want to see which L1d channels are derived in part from the subset of synthetic L1c

channels.

3 AIRS to CrIS translation

For the tests here we start with a set of atmospheric profiles and calculate upwelling radiance at a 0.0025 cm^{-1} grid with kcarta. This is convolved with SRFs for the AIRS L1c channel set to get AIRS reference truth, which we refer to as “true AIRS”. Depending on the test we may also convolve the 0.0025 cm^{-1} radiances with CrIS or other SRFs to get “true CrIS” or other reference truth.

For the CrIS standard resolution mode the channel spacing is 0.625 cm^{-1} for the LW, 1.25 cm^{-1} for the MW, and 2.5 cm^{-1} for the SW bands. The first step in the AIRS L1c to CrIS translation is to deconvolve the AIRS channel radiances to the 0.1 cm^{-1} intermediate grid, the nominal AIRS SRF resolution. Then for each CrIS band, we

- find the AIRS and CrIS band intersection
- apply a bandpass filter to the deconvolved AIRS radiances to restrict them to the intersection, with a rolloff outside the intersection
- reconvolve the filtered spectra to the CrIS user grid

Translations are validated by comparison with calculated reference truth. For the results presented in this section we start with 49 fitting profiles spanning a significant range of atmospheric conditions [3, 5]. Upwelling radiance is calculated at a 0.0025 cm^{-1} grid with kcarta [4] over a band spanning the AIRS and CrIS response functions. “True AIRS” is calculated by convolving the kcarta radiances with AIRS SRFs, and “true CrIS” by convolving kcarta radiances to a sinc basis at the CrIS user-grid specifications. AIRS is then translated to CrIS to get “AIRS CrIS”, and this is compared with true CrIS. This validation assumes perfect knowledge of the AIRS and CrIS instrument response functions and so gives only a lower bound on residuals, and on how well the translations can work in practice. The better we know the response functions, the closer real translations can approach these limits.

Figures 6, 7, and 8 show the mean and standard deviation of true CrIS minus AIRS CrIS for the 49 fitting profiles, with and without Hamming apodization, for each of the CrIS bands. Figures 9 and 10 summarize the mean and standard deviation of the residuals for Hamming apodized radiances. The residual has a high frequency component with a period of 2

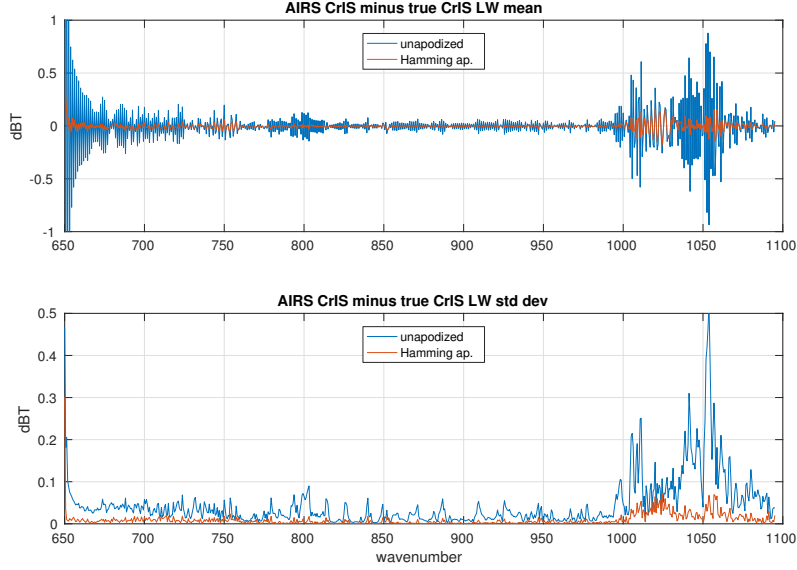


Figure 6: Mean and standard deviation of unapodized and Hamming apodized AIRS CrIS minus true CrIS, for the CrIS LW band

channel steps that is significantly reduced by the apodization. The constant or DC bias (the mean of the residuals over frequency) is very close to zero for the apodized residuals: 0.002 K for the LW, -0.005 K for the MW, and 0.001 K for the SW.

Deconvolution is significantly better than interpolation for the AIRS to CrIS translation. We consider two cases. For the first, start with true AIRS and interpolate radiances directly to the CrIS user grid with a cubic spline. For the second, interpolate true AIRS to the 0.1 cm^{-1} intermediate grid with a cubic spline and then convolve this to the use CrIS user grid. Figure 11 shows interpolated CrIS minus true CrIS for the LW band, without apodization. The two-step interpolation works a little better than the simple spline, but both residuals are significantly larger than for the translation with deconvolution. Results for the MW are similar, while the unapodized comparison is less clear for the SW. With Hamming apodization, the residuals with deconvolution are significantly less than interpolation for all three bands.

Residuals for the AIRS to apodized CrIS translation are already small, and have no significant DC bias. But there is some regularity in the residual, including an oscillation with period two channel steps. We show that a linear

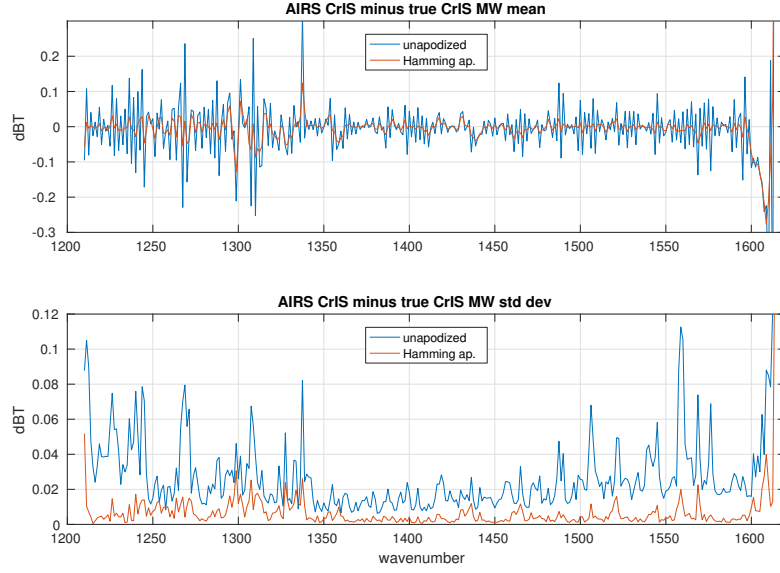


Figure 7: Mean and standard deviation of unapodized and Hamming apodized AIRS CrIS minus true CrIS, for the CrIS MW band

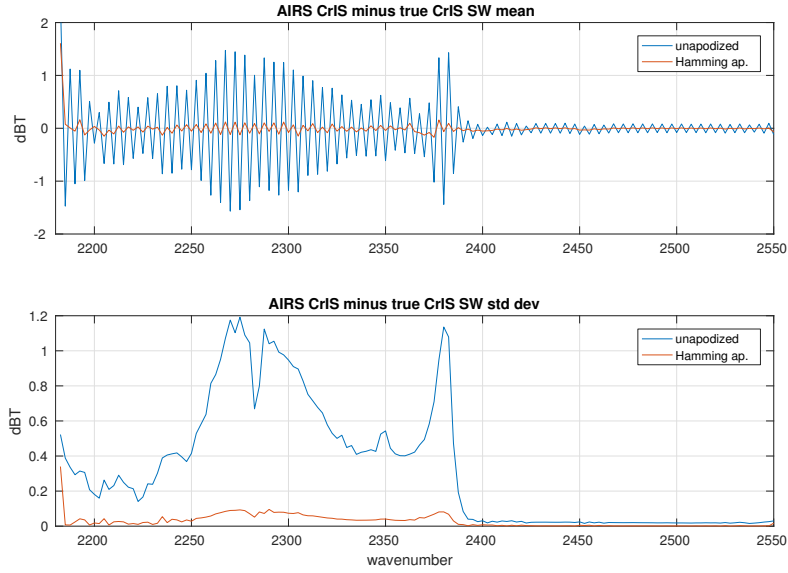


Figure 8: Mean and standard deviation of unapodized and Hamming apodized AIRS CrIS minus true CrIS, for the CrIS SW band

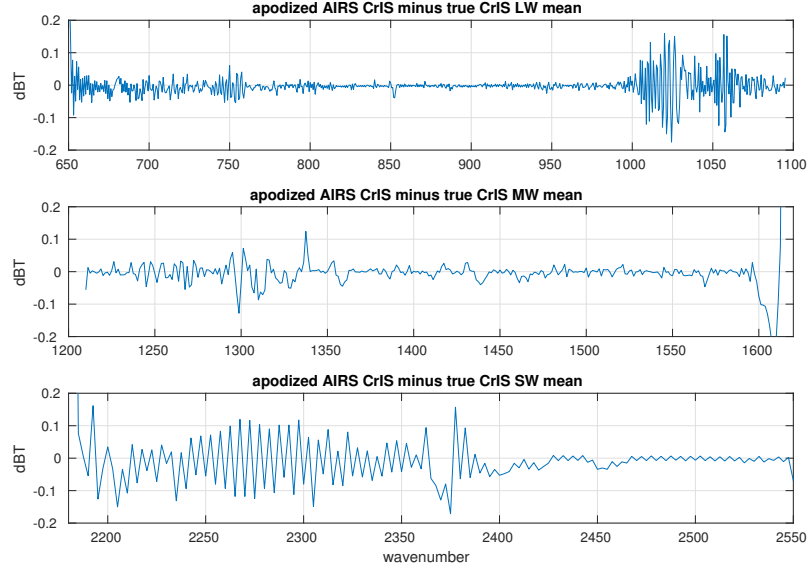


Figure 9: Mean of apodized residuals for all three CrIS bands

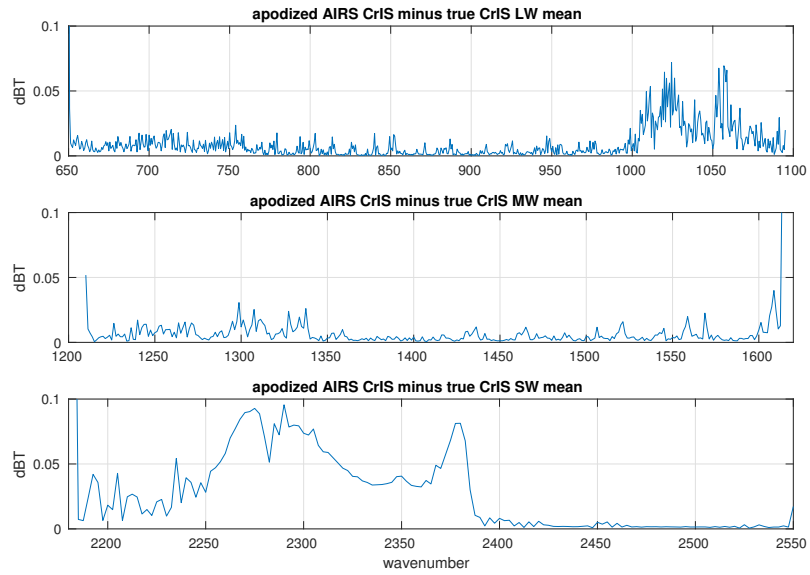


Figure 10: Standard deviation of apodized residuals for all three CrIS bands

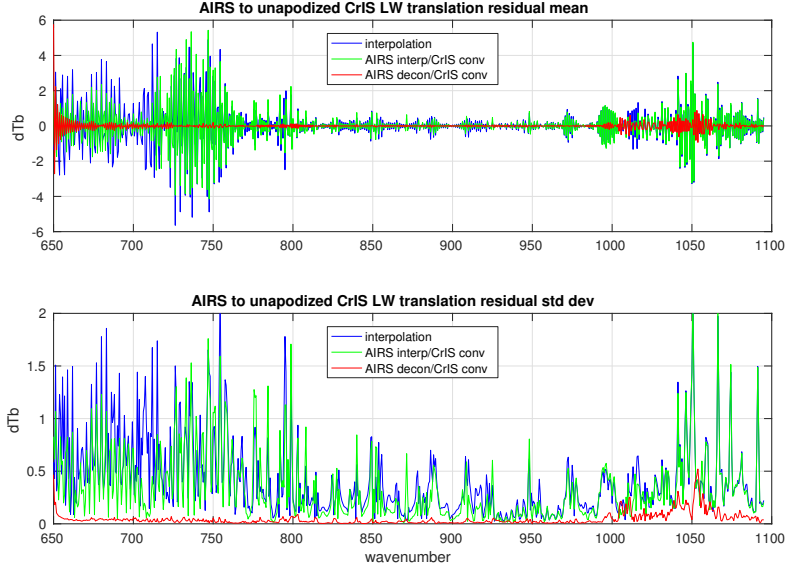


Figure 11: spline interpolation, interpolation with convolution, and deconvolution with convolution for the CrIS LW band

correction can significantly reduce this residual. This is a standard technique but worth describing briefly because the reduction is significant.

For these tests we start with kcarta radiances calculated from a set of 7377 radiances calculated from mostly cloudy AIRS profiles, spanning several consecutive days. These are split randomly into dependent and independent sets. Bias or regression coefficients are taken from the dependent set, and tests are done on the independent set. As with the 49 profile set “true AIRS” channel radiances are calculated by convolving with AIRS SRFs and “true CrIS” by convolving to the CrIS instrument specifications.

Note the difference in statistical approaches here and in section 3. There we used a small, largely uncorrelated set of 49 profiles chosen to span all common clear atmospheric conditions, and intended for developing and testing radiative transfer codes. For the statistical correction we use a more typical mix of clear and cloudy data spanning several days, moderately correlated, and large enough to allow for partition into significant dependent and independent sets.

Figure 12 is a comparison of bias, linear, and quadratic corrections for a representative dependend/independent partition. The residuals vary with the partition but the standard deviation is consistently significantly less for the linear and quadratic cases. The linear and quadratic corrections are

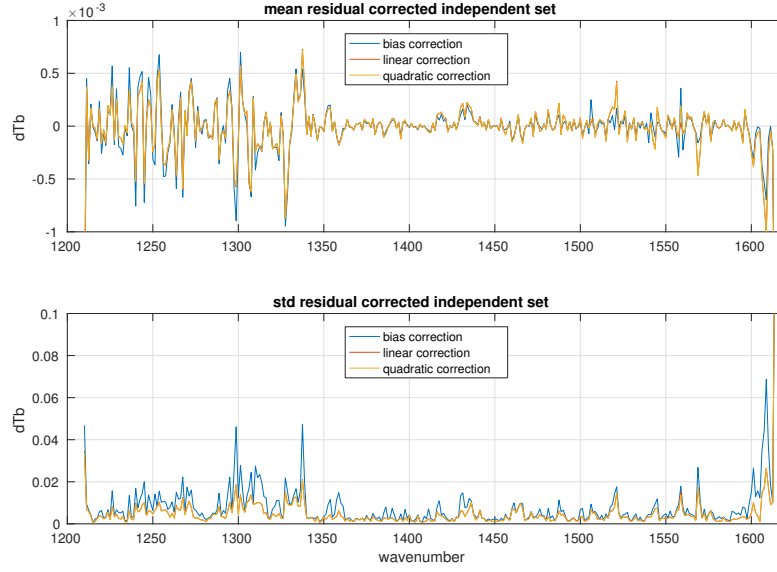


Figure 12: Mean and standard deviation of LW corrected apodized residuals for the independent subset of the 7377 profile set

nearly identical, the quadratic coefficient is very close to zero. Figure 13 shows the weights for the linear fits shown above. The a weight is very close to 1 and the b weight to earlier bias values.

Figures 14 and 15 show the linear correction is giving a similar significant improvement in the MW standard deviation in comparison with the LW, and a small improvement in the SW. As in the LW the mean residuals vary significantly depending on the dependent/independent partition, but the standard deviations are relatively stable.

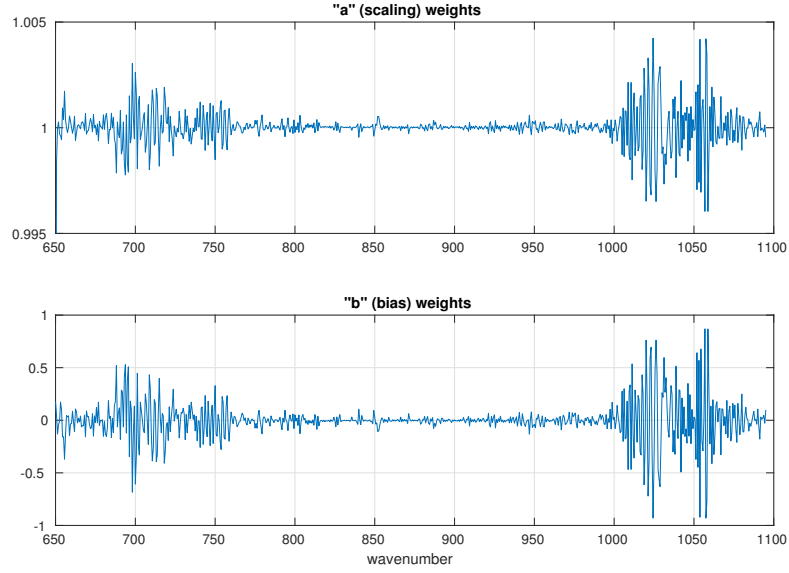


Figure 13: LW a and b weights for the linear correction $ax + b$

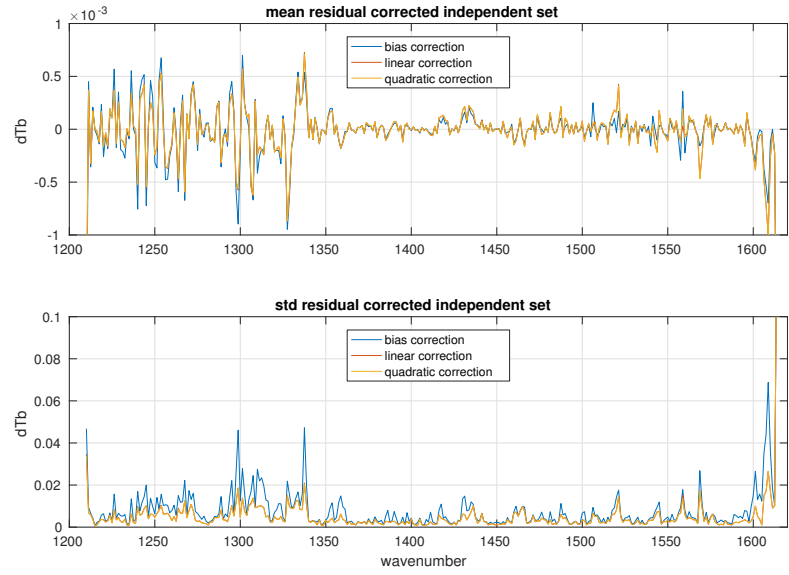


Figure 14: Mean and standard deviation of MW corrected apodized residuals for the independent subset of the 7377 profile set

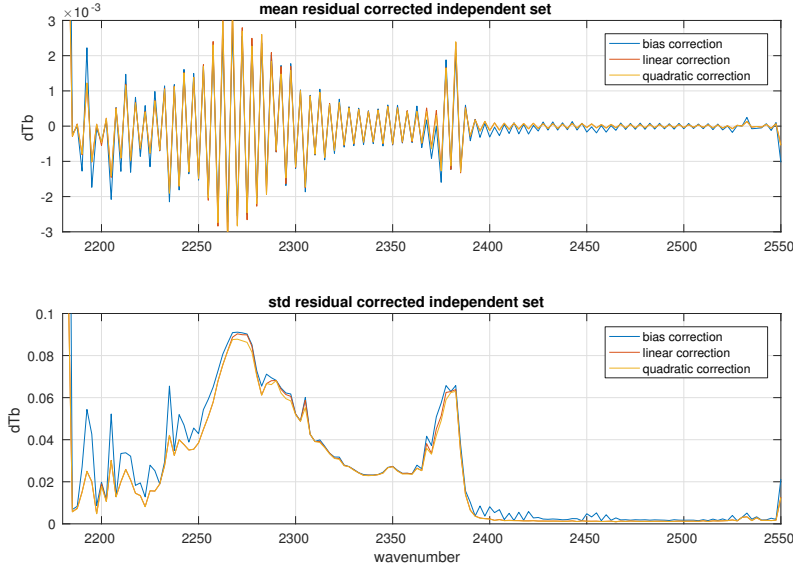


Figure 15: Mean and standard deviation of SW corrected apodized residuals for the independent subset of the 7377 profile set

4 Alternate Translations

In the remainder of this section we consider reconvolution to idealized grating instruments with resolving power of 1200 and 700. Define an AIRS L1d basis with the generalized Gaussian response function above, with $\text{FWHM} = v/\text{resolving power}$ and $dv = \text{FWHM}/2$, and with the dv -spaced channel steps starting at v_0 . In contrast with the regular spacing used for the 0.1 cm^{-1} intermediate grid, this is not oversampled.

Figure 16 shows residuals for reconvolution to an L1d basis with resolving power of 1200, the nominal AIRS resolution and figure 17 shows residuals for a resolving power of 700, half the best AIRS resolving power of 1400 in the LW. Note the different x-axes in the two figures. The uncorrected residuals are for the deconvolution/reconvolution transform “L1C to D” minus “true L1D”, Resolution is lost in shifting channel centers to a single regular function of frequency. The L1d residuals depend in part on the starting channel, and so on how the SRF peaks line up with the L1c set. The residuals above are the result of a rough fit for v_0 . For a resolving power of 1200 this gave v_0 equal to the first L1c channel, while for 700 it was the first L1c channel plus 0.2 cm^{-1} .

The residuals are reduced significantly with a linear correction. This is

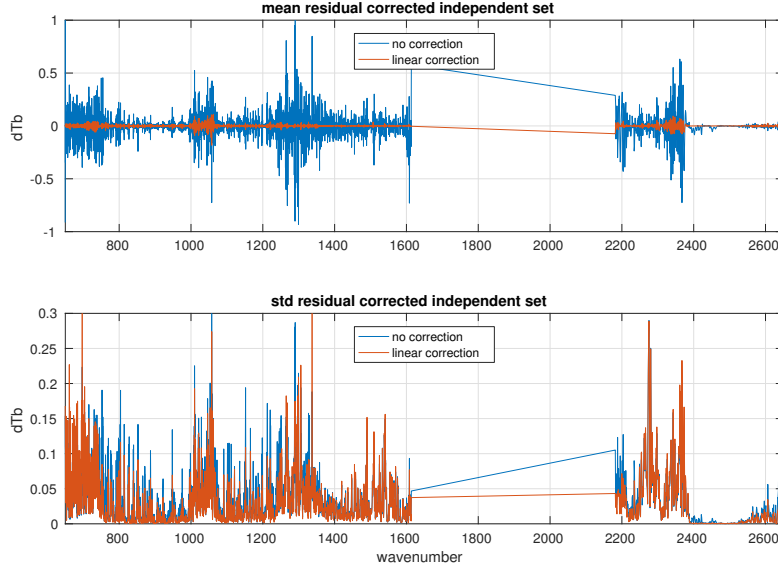


Figure 16: mean and standard deviation over the 49 fitting profiles for the L1c to L1d translation minus true L1d for a resolving power of 1200

discussed in more detail in the next section. But the key idea is to fit for a separate linear correction for each channel using a large mostly cloudy dependent set, and then use the 49 profile fitting set—the same set we are using for most other tests here—as the independent set. The separate functions guarantee no cross correlations are introduced, and the fitting profile test is more strict than for example splitting the cloudy set into dependent and independent sets, in the sense that the fitting profiles are less correlated and the residuals for the fitting set are larger.

The L1c to L1d translation can be represented as a single linear transform $S_d \cdot S_c^{-1}$, where S_c and S_d are the transforms taking the intermediate grid to L1c and L1d channels and S_c^{-1} the pseudo-inverse of S_c , that is, the deconvolution transform. We can get such a transform in other ways, for example by regression to find X that minimizes the residual $\|Xr_c - r_d\|_2$ for L1c and L1d radiance sets r_c and r_d . If r_c and r_d are m and n by k matrices, then if $k \leq m$ we can simply solve for X . If $k < m$ the system is underdetermined; in this case the residual is zero but extrapolation behavior is typically poor. If $k > m$ we can find X by regression, and extrapolation behavior can be quite good if we regress against large sets of representative data. In practice this seems to work very well, at least for minimizing

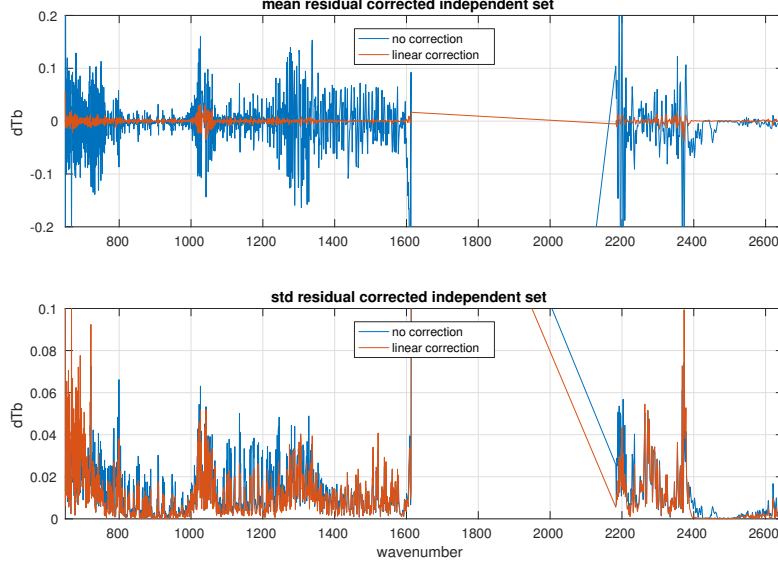


Figure 17: mean and standard deviation over the 49 fitting profiles for the L1c to L1d translation minus true L1d for a resolving power of 1200

both dependent and independent set residuals. But in contrast with the sharply banded composite transform $S_d \cdot S_c^{-1}$ the resulting transform is full of unexpected correlations and so may not be suitable for applications where we want to trace channel dependencies in the translation.

Despite the resolution loss, deconvolution is significantly better than interpolation for the L1c to L1d translation. We consider two cases. For the first, start with true L1c and interpolate radiances directly to the L1d grid with a cubic spline. For the second, interpolate true L1c to the 0.1 cm^{-1} intermediate grid with a cubic spline and convolve this to the L1d channel set. Figure 18 shows interpolated L1d minus true L1d. The two-step interpolation works a little better than the simple spline, but is still much larger than the residual for translation with deconvolution.

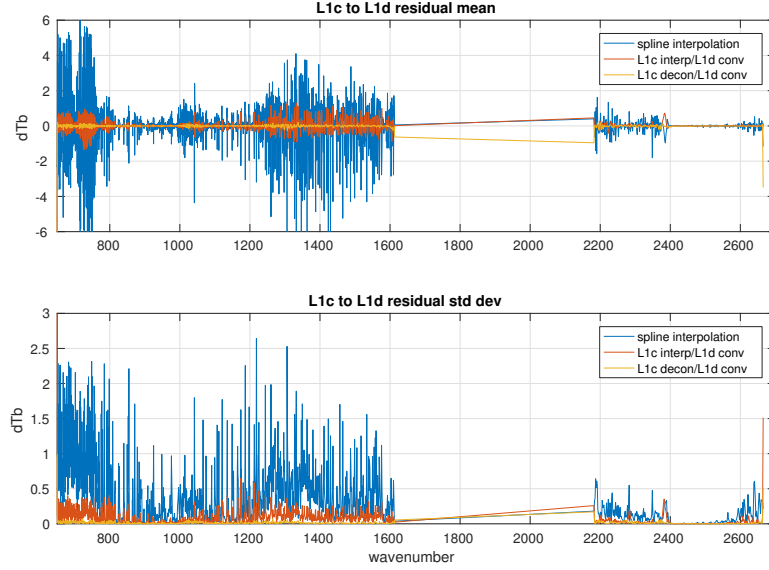


Figure 18: spline interpolation, interpolation with convolution, and deconvolution with convolution for the AIRS L1c to L1d translation with $\nu_0 = 649.822 \text{ cm}^{-1}$ and a resolving power of 700

5 Applications and conclusions

References

- [1] H. H. Aumann, M. T. Chahine, C. Gautier, M. D. Goldberg, E. Kalnay, L. M. McMillin, H. Revercomb, P. W. Rosenkranz, W. L. Smith, D. H. Staelin, L. L. Strow, and J. Susskind. AIRS/AMSU/HSB on the aqua mission: design, science objectives, data products, and processing systems. *IEEE Transactions on Geoscience and Remote Sensing*, 41:253–264, Feb. 2003.
- [2] Y. Han, H. Revercomb, M. Crompt, D. Gu, D. Johnson, D. Mooney, D. Scott, L. Strow, G. Bingham, L. Borg, Y. Chen, D. DeSlover, M. Esplin, D. Hagan, X. Jin, R. Knuteson, H. Motteler, J. Predina, L. Suwinski, J. Taylor, D. Tobin, D. Tremblay, C. Wang, L. Wang, L. Wang, and V. Zavyalov. Suomi NPP CrIS measurements, sensor data record algorithm, calibration and validation activities, and record data quality. *Journal of Geophysical Research (Atmospheres)*, 118:12734, Nov. 2013.

- [3] L. Strow, S. Hannon, S. De Souza-Machado, H. Motteler, and D. Tobin. An overview of the airs radiative transfer model. *Geoscience and Remote Sensing, IEEE Transactions on*, 41(2):303–313, Feb 2003.
- [4] L. Strow, H. E. Motteler, R. G. Benson, S. E. Hannon, and S. D. Souza-Machado. Fast computation of monochromatic infrared atmospheric transmittances using compressed look-up tables. *Journal of Quantitative Spectroscopy and Radiative Transfer*, 59(35):481 – 493, 1998. Atmospheric Spectroscopy Applications 96.
- [5] L. L. Strow, S. E. Hannon, S. De-Souza Machado, H. E. Motteler, and D. C. Tobin. Validation of the atmospheric infrared sounder radiative transfer algorithm. *Journal of Geophysical Research: Atmospheres*, 111(D9), 2006. D09S06.
- [6] L. L. Strow, H. Motteler, D. Tobin, H. Revercomb, S. Hannon, H. Buijs, J. Predina, L. Suwinski, and R. Glumb. Spectral calibration and validation of the Cross-track Infrared Sounder on the Suomi NPP satellite. *Journal of Geophysical Research (Atmospheres)*, 118:12486, Nov. 2013.